Received: 7 August 2018 | Revised: 20 September 2018 | Accepted: 10 October 2018

DOI: 10.1002/ese3.252

RESEARCH ARTICLE

Energy Science & Engineering Open Access

Multi-objective performance optimization of irreversible molten carbonate fuel cell–Stirling heat engine–reverse osmosis and thermodynamic assessment with ecological objective approach

Mohammad H. Ahmadi[1] | **Mohammad Sameti**[2] | **Seyed M. Pourkiaei**[3] | **Tingzhen Ming**[4] | **Fathollah Pourfayaz**[3] | **Ali J. Chamkha**[5,6] | **Hakan F. Oztop**[7] | **Mohammad Ali Jokar**[3]

[1]Faculty of Mechanical Engineering, Shahrood University of Technology, Shahrood, Iran

[2]Faculty of Engineering and Computer Sciences (ENCS), Concordia University, Montreal, Quebec, Canada

[3]Department of Renewable Energy and Environmental Engineering, University of Tehran, Tehran, Iran

[4]School of Civil Engineering and Architecture, Wuhan University of Technology, Wuhan, China

[5]Mechanical Engineering Department, Prince Sultan Endowment for Energy and Environment, Prince Mohammad Bin Fahd University, Al-Khobar, Saudi Arabia

[6]RAK Research and Innovation Center, American University of Ras Al Khaimah, Ras Al Khaimah, United Arab Emirates

[7]Department of Mechanical Engineering, Technology Faculty, Fırat University, Elazig, Turkey

Correspondence
Mohammad H. Ahmadi, Faculty of Mechanical Engineering, Shahrood University of Technology, Shahrood, Iran
Emails: mohammadhosein.ahmadi@gmail.com, mhosein.ahmadi@shahroodut.ac.ir
and
Hakan F. Oztop, Department of Mechanical Engineering, Technology Faculty, Fırat University, Elazig, Turkey
Email: hfoztop1@gmail.com

Funding information
National Natural Science Foundation, Grant/Award Number: 51778511; Hubei Provincial Natural Science Foundation, Grant/Award Number: 2018CFA029; Key Project of ESI Discipline Development of Wuhan University of Technology, Grant/Award Number: 2017001; Scientific Research Foundation of Wuhan University of Technology, Grant/Award Number: 40120237

Abstract

This paper aims to investigate a hybrid cycle consisting of a molten carbonate fuel cell (FC) and a Stirling engine which, by connecting to a seawater reverse osmosis desalination unit, provides fresh water. First, a parametric evaluation is performed to study the effect of some key parameters, including the current density and the working temperature of the FC and the thermal conductance between the working substance and the heat reservoirs in the Stirling engine, on the objective functions. The objective functions include the energy efficiency, the exergy destruction rate density, the fresh water production rate, and the ecological function density. After investigating each double combination of these objective functions, two scenarios are defined in quest to concurrently optimize three functions together. The first scenario aims to optimize the energy efficiency, the exergy destruction rate density, and the fresh water production rate; and the second scenario attempts to optimize the energy efficiency, the fresh water production rate, and the ecological function density. A multi-objective evolutionary algorithm joined with the nondominated sorting genetic algorithm (NSGA-II) approach is employed to obtain Pareto fronts in each case scenario. In order to ascertain final solutions between Pareto fronts, three fast and robust decision-making methods are employed including TOPSIS, LINMAP, and Fuzzy. Finally, a sensitivity analysis is conducted to critically analyze the performance of the system.

KEYWORDS
molten carbonate fuel cell, multi-disciplinary approach, multi-objective optimization, reverse osmosis desalination, stirling engine

1 | INTRODUCTION

Stirling cycle is one of the most common air cycles for heat engines. The advantages of the cycle include the specific efficiency and the ability to use different types of fuels for different heating purposes. In theory, the Stirling engine can transform heat into work with a high efficiency when isothermal expansion and compression and ideal regeneration are applied (Carnot efficiency). The cold and hot temperatures of the cycle are determinative for the thermal limitation of the operational condition in Stirling engine. Generally, the cold and hot temperatures of the Stirling engine are 338 and 925 K, respectively.[1] Stirling engine performance could be varied from 30% to 40% corresponding to a temperature range of 923-1073 K.[2,3] Combination of solar collectors and Stirling engines is a modern technique which provides ease of power generation.

There are four various categories of concentrated solar power (CSP) plants: Linear Fresnel Reflectors, Parabolic Troughs, Power Tower, and Stirling Dish systems. Although the aforementioned systems have different setups, their primary apparatus are similar; Being based on concentration of solar radiation onto a small area. In CSP plants systems, the Stirling dish has the maximum efficiency about 27%.[4] Dish-Stirling system arrangements are represented in Refs 5-7. In the past 20 years, eight different dish-Stirling configurations were developed by companies in Germany, the United States, Russia, and Japan.[8] A 1.5 MW capacity installation is currently under construction at Peoria, AZ, and multi-hundred megawatts capacity plants have been designed and are in progress.[9] There are some 9-10 MW capacity plants in India and additional high capacity plants in the United States (750-850 MW).[10]

Recently, many studies have been carried out to determine the optimal performance of solar-driven energy systems, using the finite-time thermodynamic (FTT) analysis.[11-27] The answers obtained by the FTT are more consistent than other thermodynamic methods. Lund[11] defined parametric equations to describe these conditions for a solar thermal power plant in terms of rate of reversible finite heat transfer. Ibrahim and Ladas[14] obtained a finite-time parameter to enhance the heat transfer specifications of a Stirling engine. Blank et al[15] studied and optimized an actual endoreversible Stirling engine. Trukhow et al[17] investigated the equivalence of energy of a solar power plant coupled with a Stirling engine and showed that the generated electricity is subjected to the solar radiation direction. Chen et al[18] studied the efficiency of a solar Stirling engine at the maximum electricity generation rate. Yilmaz et al[24] have obtained the aforementioned conditions for a Carnot-type irreversible solar-powered heat engine. Yaqi et al[26] applied FTT to regulate optimum operational condition of a solar-powered Stirling heat engine.

Earlier, fuel cells (FCs) have been investigated in numerous studies due to growing environmental pollution, climate changes, and reducing fossil resources. As well as being zero emission, having high efficiency, and consistent facilities, FCs could be combined with various thermal cycles. Different models of FCs are studied and investigated in the literature. Still, these setups can be evaluated from different aspects. Thermodynamic assessment and numerical study are known as main efficiency analysis tools for these thermal cycles.[28-34] Zhao et al[28] represented a thermodynamic approach to investigate an irreversible solid oxide fuel cell (SOFC), by the mean of nonequilibrium thermodynamics. Zhang et al[30] studied molten carbonate fuel cell (MCFC) and employed a multi-optimization method aiming the energy efficiency and power output simultaneously.

In line with the progression of FC technology, various approaches have been developed. Hybridization of FCs is one of the aforementioned approaches which recovers rejected heat of high temperature to enhance the overall performance. Various arrangements of FC-heat engines setups are feasible.[35-51] SOFC and MCFC which operate at high temperatures are more suitable for these purposes. Zhang et al[37] designed a model for a hybrid MCFC-heat engine setup, and evaluated the effective parameters on the system efficiency. Moreover, a MCFC-GT arrangement was optimized and investigated by defining the performance and efficiency.[39] Chen et al[41] investigated a MCFC-Stirling engine and studied the performance enhancement due to coupling. Similarly, they studied the affective operational parameters of the system and their impact on the performance. To recover the waste heat produced by MCFCs, Yang et al[47] proposed a new model to investigate an MCFC-themophotovotaic cell (TPVC) hybrid system which revealed the advantages of the potential cycle. The current density of the MCFC, voltage output of the TPVC, electrode area ratio of the MCFC to the TPVC, and energy gap of the material in the photovoltaic cell were considered as the decision variables to optimize the power output and the efficiency

of the hybrid cycle. For a similar purpose, Ye et al[51] proposed a hybrid system consisting of an MCFC, a regenerator and a thermoradiative cell (TRC) with similar objective functions. They showed that the TRC can be coupled with other high-temperature fuel cells (HTFCs), like SOFC and direct carbon fuel cell, to utilize the waste heat released by the HTFCs more effectively.

Evolutionary algorithms (EAs) were developed since the mid-1980s in order to help clarify this wide-ranging type of multi-objective issues.[52] Generally, EA specify a collection of satisfying answers, with no overlaps.[53] Generally, in multi-objective optimization problems, a numerous set of answers called Pareto frontier is examined, to represent the closest match in the objective function area. On this subject, researchers have evaluated multi-objective optimization for different energy systems in order to determine the best optimal operation conditions of the system.[54-90]

In the present paper, an irreversible thermodynamic-electrochemical model of a MCFC-Stirling heat engine-RO hybrid system is established, in which not only the irreversible losses in the MCFC but also the heat-leak from the FC to the environment as well as heat transfer between the FC and the heat engine are considered.

2 | MODEL DESCRIPTION

2.1 | MCFC model

The discussion of different aspects of the MCFC is beyond the scope of this research. However, a brief description of the cycle in thermodynamics point of view is provided here. Natural gas is converted to hydrogen in a reformer. Then a mixture of water vapor and natural gas is preheated in a heat exchanger and fed to the reformer. The required heat for the reforming reactions is supplied by the catalytic burner which burns the anode outlet in an air stream, which is preheated by part of cathode exhaust gases. The air stream provides the required amount of oxygen for the electrochemical reaction at the cathode side and further combustion of the fuel. The reformer outlet stream preheats the inlet steam and is cooled to the desired temperature, and enters the anode where it takes part in an electrochemical reaction. The anode outlet gas mixes with air and enters the catalytic burner. The high temperature outlet stream of the burner is a significant source of heat and provides the heat needed to allow the bottom cycle to attain the required performance. After the stream is fed to cathode, the carbonate ion produced at the cathode side is transferred to the anode side. The cathode exhaust gases contain a large amount of thermal energy which is used for preheating the inlet air stream and supplying the steam needed by the reformer, because the overall temperature of the FC should maintain constant and also the temperature of the reactants is lower than the needed working temperature by the FC. The performance of MCFCs from different points of view and in more detail are studied in Refs 30,39,41,47,48,51.

Anode potential (U_{an}), cathode potential (U_{cat}), ohm overpotential (U_{ohm}), and theoretical maximum potential (U_t) of MCFC can be calculated as follows, respectively[91]:

$$U_{an} = 2.27\times10^{-9} j e^{\left(\frac{En_{act,an}}{RT}\right)} p_{H_2,an}^{-0.42} p_{CO_2,an}^{-0.17} p_{H_2O,an}^{-1} \quad (1)$$

$$U_{cat} = 7.505\times10^{-10} j e^{\left(\frac{En_{act,cat}}{RT}\right)} p_{O_2,cat}^{-0.43} p_{CO_2,cat}^{-0.09} \quad (2)$$

$$U_{ohm} = 0.5\times10^{-4} j e^{(3016(\frac{1}{T}-\frac{1}{923}))} \quad (3)$$

$$U_t = U_i + \frac{RT}{n_e F}\ln\left(\frac{p_{H_2,\,an}\left(p_{O_2,\,cat}\right)^{0.5} p_{CO_2,\,cat}}{p_{H_2O,\,an} p_{CO_2,\,an}}\right) \quad (4)$$

where, j is the current density, $p_{H_2,\,an}$ is the partial pressure of hydrogen at the anode, $p_{CO_2,\,an}$ is the partial pressure of carbon dioxide at the anode, $p_{H_2O,\,an}$ is the partial pressure of water at the anode, $p_{O_2,\,cat}$ is the partial pressure of oxygen at the cathode, $p_{CO_2,\,cat}$ is the partial pressure of carbon dioxide at the cathode, R is the universal gas constant, T is the operating temperature of the MCFC, En_{act} is the activation energy, F is the Faraday constant, n_e is the number of electrons, and U_i is the ideal standard potential.

$$U_i = \frac{-\Delta g^0}{n_e F} \quad (5)$$

Cell voltage is written by using Equations (1)-(5):

$$U_{cell} = (U_t - U_{an} - U_{cat} - U_{ohm}) \quad (6)$$

Power and efficiency of the FC are:

$$P_C = U_{cell} jA \quad (7)$$

$$\eta_C = \frac{P_C}{-\Delta\dot{H}} \quad (8)$$

where $-\Delta\dot{H}$ is the maximum possible power from the FC and it can be described as:

$$-\Delta\dot{H} = -\frac{jA\Delta h}{n_e F} \quad (9)$$

where, A is the area of the interconnect plate and Δh is the molar enthalpy change. Exergy destruction rate of FC is:

$$Exd_C = \left(-\frac{\Delta h}{n_e F} - U_{cell}\right) jA \quad (10)$$

Regenerative loss in the regenerator can be described as:

$$\dot{Q}_r = K_r(1-\varepsilon_r)(T-T_0) \quad (11)$$

where, K_r is the heat conductance of the regenerator, ε_r is the regenerator efficiency, and T_0 is the environment temperature. Heat input to the bottom cycle is written as Equation (12):

$$\dot{Q}_h = -\Delta\dot{H} - P_C - \dot{Q}_r \tag{12}$$

2.2 | Analysis of the Stirling engine

Ideal Stirling cycle consists of four processes including two isothermal and two isochoric processes in the regenerator. In a real cycle, it is impractical to have an ideal heat transfer in the regenerator, in which the entire amount of absorbed heat is transferred to the working fluid in the isochoric heating process. Therefore, a heat transfer loss occurs in the regenerator. In addition, a conductive heat transfer occurs between the heat source and sink, namely conductive thermal bridge loss. More details on the Stirling engines and how they work can be found in previous works.[1,34,58,59,62-65,69,77,83,89,92] In the next step, the thermodynamic parameters of this system must be calculated. Equations (11) and (12) are representing the heat transfer in the cycle. Heat inputs are:

$$Q_h = \theta(T - T_1)t_1 \tag{13a}$$

$$Q_h = nRT_1 \ln x \tag{13b}$$

Heat outputs are:

$$Q_l = \theta(T_2 - T_L)t_2 \tag{14a}$$

$$Q_l = \mathrm{nRT}_2 \ln x \tag{14b}$$

where θ is the heat conductance (W m^{-2} K^{-1}), n is the mole number, x is the compression ratio ($x = V_{max}/V_{min}$), T_1 and T_2 are average temperatures of the compression and expansion processes, and t_1 and t_2 are the times spent on the two isothermal branches. Applying Equations (13) and (14) will provide t_1 and t_2. T_1 is calculated by applying Equations (12) and (13a).

Regenerative loss is:

$$\Delta Q_r = \alpha nC(T_2 - T_L)t_2 \tag{15}$$

where C is the heat capacity (J mol^{-1}), α is the imperfect regeneration coefficient. Time spent on regeneration time is:

$$t_r = b(t_2 + t_1) \tag{16}$$

Heat rate can be obtained as:

$$\dot{Q}_h = \frac{\ln x + \frac{\alpha(1-y)}{(\delta-1)}}{(1+b)\left(\frac{\ln x}{\theta(T-T_1)} + \frac{y \ln x}{\theta(yT_1 - T_L)}\right)} \tag{17}$$

Using Equations (12) and (17), x can be defined. Energy efficiency of the irreversible Stirling cycle can be described as:

$$\eta_S = 1 - \frac{\dot{Q}_l}{\dot{Q}_h} = \frac{1-y}{1 + \frac{\alpha(1-y)}{(\delta-1)\ln x}} \tag{18}$$

where δ is the ratio of the specific heats, and heat rejection from the irreversible Stirling engine is obtained by using Equation (18):

$$\dot{Q}_l = \dot{Q}_h(1 - \eta_S) \tag{19}$$

Power and exergy destruction rate of the irreversible Stirling engine are shown respectively in Equations (20)-(21):

$$P_S = \dot{Q}_h - \dot{Q}_l \tag{20}$$

$$\mathrm{Exd}_S = T_0\left(\frac{\dot{Q}_l}{T_l} - \frac{\dot{Q}_h}{T}\right) \tag{21}$$

Power output, energy efficiency, and exergy destruction rate density of the hybrid system are described in Equations (23-24), respectively:

$$P_H = P_C + P_S \tag{22}$$

$$\eta_H = \frac{P_C + P_S}{-\Delta\dot{H}} \tag{23}$$

$$\mathrm{exd}_H = \frac{\mathrm{Exd}_C + \mathrm{Exd}_S}{A} \tag{24}$$

In the next step the environmental criteria are investigated. The ecological function is defined by the difference of power output and exergy destruction created by the entropy generation. This function can enhance the power output so long as decreasing exergy destruction which leads to lower environmental side-effects.

$$E_H = P_H - \mathrm{Exd}_H \tag{25}$$

$$e_H = \frac{E_H}{A} \tag{26}$$

2.3 | Reserve osmosis desalination subsystem

Reverse Osmosis, commonly referred to as RO is one of the leading methods for fresh water production which is based on the selective permeability. Reverse osmosis process involves the movement of water through the membrane, opposed to the concentration gradient (from low to high). Furthermore, a pressure is applied on the concentrated side in order to prevail osmotic pressure. Dessouky[93] have presented a numerical model for the RO arrangement.

The mass and salt balances are given by

$$\dot{m}_f = \dot{m}_p + \dot{m}_b \tag{27}$$

$$x_f\dot{m}_f = x_p\dot{m}_p + x_b\dot{m}_b \tag{28}$$

where $\dot{m}_f$, $\dot{m}_p$, and $\dot{m}_b$ are the feed flow rate, the permeate flow rate, the brine flow rate, respectively and x_f, x_p, x_b are the feed salinity, the permeate salinity, the brine salinity.

The feed water mass flow rate $\dot{m}_f$ based on the recovery ratio R_R, whose value we chosen is 0.3, and the fresh water mass flow rate $\dot{m}_p$ is

$$\dot{m}_f = \frac{\dot{m}_p}{R_R} \tag{29}$$

The mass flow rate of water passage through a semipermeable membrane is given by:

$$\dot{m}_p = (\Delta p - \Delta \pi) K_w A_m \tag{30}$$

where A_m is the area of reserve osmosis membrane, K_w is the water permeability coefficient, which is expressed as

$$K_w = \frac{6.84 \times 10^{-8} \times (18.68 - (0.177 \times x_b))}{T_f} \tag{31}$$

where T_f is the temperature of feed water.
Δp is the permeate hydraulic and $\Delta \pi$ is the osmotic pressure, and they can be expressed by

$$\Delta p = \bar{p} - p_p \tag{32}$$

$$\Delta \pi = \bar{\pi} - \pi_p \tag{33}$$

where p_p and π_p are the hydraulic and osmotic pressures of the permeate stream, respectively. $\bar{p}$ and $\bar{\pi}$ are the average feed water pressure and average osmotic pressures on the feed side and brine side, which are given by

$$\bar{p} = 0.5(p_f + p_b) \tag{34}$$

$$\bar{\pi} = 0.5(\pi_f + \pi_b) \tag{35}$$

where p_f and p_b are the hydraulic pressure of feed stream and reject stream. π_f and π_b is the osmotic pressure of feed stream and reject stream.

Osmotic pressures can be expressed by

$$\pi_f = RTx_f \tag{36}$$

$$\pi_b = RTx_b \tag{37}$$

$$\pi_p = RTx_p \tag{38}$$

where R is the universal gas constant and T is the water temperature.

The mass flow rate of fresh water output driven by the mechanical power $P_H$is estimated as

$$P_H = \frac{\Delta p_{net} \dot{m}_f}{\rho_f \eta_{pump}} = P_C + P_{st} \tag{39}$$

where ρ_f is the feed flow rate density, η_{pump} is the driving pump mechanical efficiency, and Δp_{net} is the net pressure difference across the high pressure pump.

3 | OPTIMIZATION ALGORITHM

Generally, in multi-objective optimization problems, a numerous set of answers called Pareto frontier is provided, to represent the closest match in the objective function area.[53] Multi-objective evolutionary algorithms (MOEAs), which provide a number of solutions to estimate the Pareto optimal class, have been employed widely by researchers. It is approved that MOEAs can overcome the difficulties of regular methods.[52] In this study, the Pareto frontier is provided by applying NSGA-II approach. The principles of this method are explained in Refs 94,95.

In order to select the optimum solution from the outputs in multi-objective issues, a procedure called "decision making" is used. Several decision-making methods are available for selecting final optimum answer from Pareto front. On account of the probable dissimilar scales of objectives, the dimensions must be unified. Moreover, in decision-making procedure objectives' vectors have to be nondimensionalized. Most common nondimensionalization methods are: Fuzzy, Linear, and Euclidian. In this paper, three decision-making methods including LINMAP, TOPSIS, and Fuzzy are utilized. LINMAP and TOPSIS use the Euclidian and the Fuzzy employs the Fuzzy nondimensionalization technique. More features about decision makers and more examples of their application can be found in the previous studies.[1,62,64-68,70-72,74-79,82-85,92]

4 | RESULTS AND DISCUSSION

4.1 | Objective functions, restraints, and decision variables

In this simulation, the energy efficiency (η_H), fresh water production rate ($\dot{m}_p$), exergy destruction rate density (exd_H), and the ecological function density (e_H) are considered as the objective functions in order to optimize the performance of the proposed cycle. Three decision variables are used for this optimization. Table 1 lists these variables and their ranges which are determined by the suggestions provided in the

TABLE 1 Ranges of the decision variables in this simulation

Variable	Current density (j)	Operating temperature of the MCFC (T)	The thermal conductance between the working substance and the heat reservoir (θ)
Unit	$A.m^{-2}$	K	$W K^{-1}$
Lower bound	1000	905	900
Upper bound	7000	925	1100

TABLE 2 Values for parameters in order of appearance in the proposed model

Parameter	Unit	Value
Partial pressure of hydrogen at the anode	atm	0.6
Partial Pressure of carbon dioxide at the anode	atm	0.058
Partial Pressure of water at the anode	atm	0.342
Partial Pressure of oxygen at the cathode	atm	0.08
Partial Pressure of carbon dioxide at the cathode	atm	0.08
Activation energy at the anode	J mol^{-2}	53 500
Activation energy at the cathode	J mol^{-2}	77 300
Universal gas constant	J mol^{-1} K^{-1}	8.314
Ambient temperature	K	298.15
Faraday constant	C mol^{-1}	96 485
Number of electrons	—	2
Molar Gibbs energy change	J mol^{-1}	−197 000
Molar enthalpy change	C mol^{-1}	−247 430
Heat conductance of the regenerator	W m^{-2}	5
Interconnect plate area of the fuel cell	m^2	25
Regenerator efficiency	—	0.9
Warm seawater temperature	K	298.15
High pressure pump efficiency	—	0.80
Feed flow rate density	kg m^{-3}	1029
Net pressure difference across the pump	MPa	3
Recovery ratio	—	0.3

literature.[91,96-100] They include the current density (j) which is the most important controllable variable of the FC, working temperature of the MCFC (T), which is the maximum temperature of the hybrid cycle, and the thermal conductance between the working substance and the heat reservoirs at temperatures T_1 and T (θ). Other parameters are listed in Table 2.

The energy efficiency, fresh water production rate, and the exergy destruction rate density are the three objective functions for the first scenario, evaluated via Equations (23, 30, 24).

The energy efficiency, fresh water production rate, and the ecological function density are the three objective functions for the second scenario, evaluated via Equations (23, 30, 26).

To determine the optimal design variables of the system, based on the genetic algorithm approach, a simulation program was coded through Matlab software. Specifications of GA for optimization puzzle are reported through Table 3.

TABLE 3 Specification of GA for optimization puzzle in this paper

GA Parameters	Value
Population size	400
Population type	Double vector
Tournament size	20
Selection process	Tournament
Maximum number of generations	1000
Mutation	Restriction dependent

4.2 | Parametric evaluation of the hybrid cycle

In the first part of this analysis, the characteristic curves of the hybrid cycles are plotted (Figure 1f). This stage is of high importance because it helps understand the behavior of the cycle and also enable one to interpret the outcomes of the next part more clearly.

Figure 1a shows the variation of the energy efficiency with the dimensionless exergy destruction rate ($\sigma^* = \mathrm{exd_H} / \max(\mathrm{exd_H})$). This plot starts at $j = 1000$ (A m^{-2}), on the bottom right corner, and by increasing the current density, the energy efficiency first increases and then decreases, while the exergy destruction rate always increases. Therefore, if one wants to optimize these two targets, the answer is somewhere between the starting point and the point where the energy efficiency is maximum. Another point here is that the influence of changing decision variables is less noticeable in this region. Figure 1b depicts the variation of the energy efficiency with the dimensionless fresh water production rate ($m^* = m_p / \max(m_p)$). The curve starts on the bottom right hand corner. With an increase in the current density, the energy efficiency and the fresh water production rate both increase at first. But, then the energy efficiency starts to decrease while the fresh water production rate still increases. Finally, when the fresh water production rate passes its maximum, both targets decrease. Therefore, if the goal is to optimize these objective functions, the selected point will be somewhere between the point which maximizes the energy efficiency and the other point which maximizes the fresh water production rate. This figure also shows the fact observed before which is by increasing the current density, the influence of changing other decision variables, including the working temperature of the MCFC and the thermal conductance, will increase. Figure 1c illustrates the variation of the dimensionless fresh water production rate with the dimensionless exergy destruction rate. These curves start on the bottom left hand corner where the exergy destruction rate is minimized. Then by increasing the current density, the exergy destruction rate increases along with a

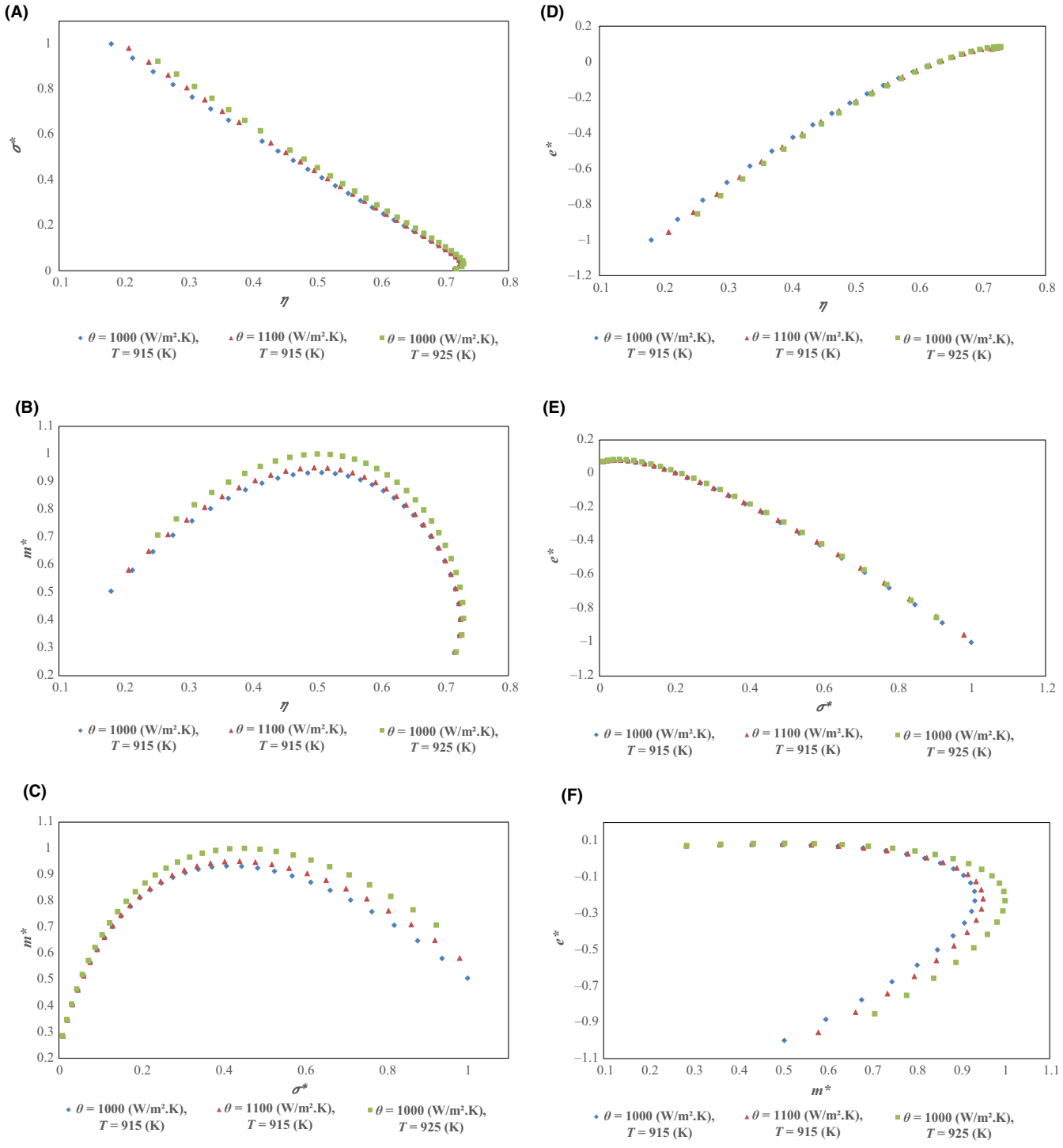

FIGURE 1 Characteristic curves of the hybrid cycle. (a) The curves of dimensionless exergy destruction rate varying with energy efficiency for different working temperatures of the MCFC and thermal conductance. (b) The curves of dimensionless fresh water production rate varying with energy efficiency for different working temperature of the MCFC and thermal conductance. (c) The curves of dimensionless fresh water production rate varying with dimensionless exergy destruction rate for different working temperature of the MCFC and thermal conductance. (d) The curves of dimensionless ecological function varying with energy efficiency for different working temperatures of the MCFC and thermal conductance. (e) The curves of dimensionless ecological function varying with dimensionless exergy destruction rate for different working temperatures of the MCFC and thermal conductance. (f) The curves of dimensionless ecological function varying with dimensionless fresh water production rate for different working temperatures of the MCFC and thermal conductance.

temporary increase in the fresh water production rate. After maximizing the fresh water production rate, the curves start to go down. Figure 1d shows the variation of the energy efficiency with the dimensionless ecological function ($e^* = e_H/\text{abs}(\min(e_H))$) . The curves start on the top right hand corner where it seems both the targets are maximized.

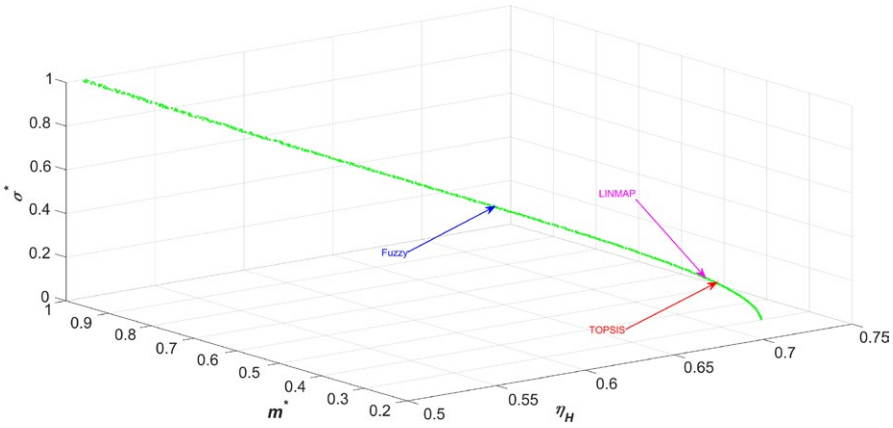

FIGURE 2 Pareto optimal frontier in the objectives' space for the first scenario

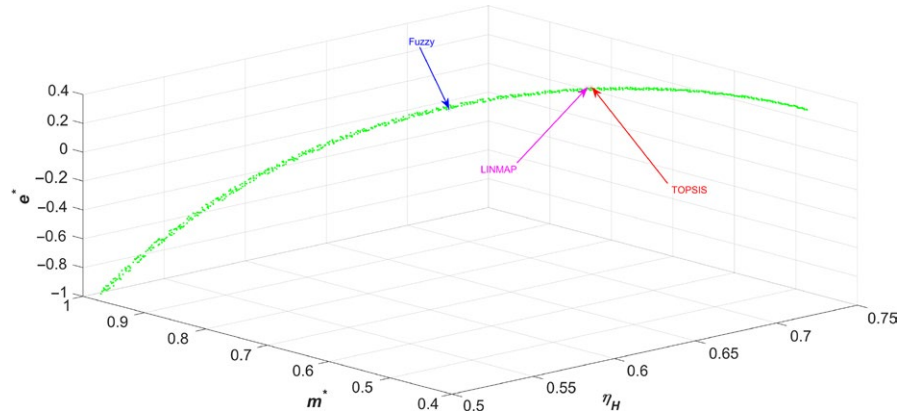

FIGURE 3 Pareto optimal frontier in the objectives' space for the second scenario

But it should be noticed that at first, the energy efficiency and the ecological function are not exactly maximized. By increasing the current density, they reach their maximum points. Another point here is that at first, increasing the working temperature of the MCFC and the thermal conductance help the ecological function and the energy efficiency but at higher current densities, it has a negative effect on the ecological function. The effect of increasing these two decision variables always has a positive effect on the energy efficiency. Figure 1e depicts the variation of the dimensionless ecological function with the dimensionless exergy destruction rate. It starts on the top right hand corner. The exergy destruction rate always increases with an increase in the current density while the ecological function first increases and then decreases. Therefore, if one aims to optimize these targets together, the answer is somewhere between the starting point and the point where the ecological function is optimized. The influence of changing other decision variables on the targets again increases along with an increase in the current density. Figure 1f illustrates the variation of the dimensionless ecological function with the dimensionless fresh water production rate. The ecological function first increases slightly along with an increase in the fresh water production rate but then decreases until the end. The figure also shows that the maximization of the fresh water production rate occurs at higher current densities compared to the energy efficiency.

4.3 | Multi-objective optimization

As shown in the proceeding section, there is a conflict between the objective functions and there is no single solution to optimize all of them concurrently. Therefore, in this step two multi-objective optimization problems are defined to try to optimize different combinations of the targets and compare the results. The first scenario is to maximize the energy efficiency and the fresh water production rate while minimizing the exergy destruction rate. In the second scenario, the exergy destruction rate density is replaced with the ecological function density. Three robust decision-making methods are employed to select the final answers between the Pareto fronts obtained by the evolution algorithm.

The Pareto optimal fronts for the first and second scenarios are shown in Figures 2 and 3, respectively. Tables 4 and 5 address the optimal outputs achieved by executing LINMAP, TOPSIS, and Fuzzy decision-making methods.

As these results show, the final outputs are located at higher working temperatures of the MCFC and also higher values of the thermal conductance. This accord with the

TABLE 4 Outcomes of the decision makers for the first scenario

Decision-making methods	Decision variables			Considered objective functions			Not-considered objective function
	j (A m^{-2})	θ (W K^{-1})	T (K)	η_H	$\dot{m}_p$ (m^3 s^{-1})	exd_H (kW m^{-2})	e_H (kW m^{-2})
TOPSIS	1515	1097.2	925	0.7299	2.918	0.4824	0.9355
LINMAP	1610	1097.9	924.83	0.7288	3.0963	0.5616	0.9429
Fuzzy	2820	1098.7	924.69	0.6807	5.0656	1.8506	0.6108
Ideal point	—	—	—	0.7302	6.7567	0.1093	0.9474
Nonideal point	—	—	—	0.0553	1.0220	14.214	−13.717

TABLE 5 Outcomes of the decision makers for the second scenario

Decision-making methods	Decision variables			Considered objective functions			Not-considered objective function
	j (A m^{-2})	θ (W K^{-1})	T (K)	η_H	$\dot{m}_p$ (m^3 s^{-1})	e_H (kW m^{-2})	exd_H (kW m^{-2})
TOPSIS	2540	1099.4	925	0.6962	4.6664	0.7667	1.5007
LINMAP	2560	1098	924.99	0.6952	4.6961	0.7573	1.5246
Fuzzy	3185	1098.2	923.11	0.6559	5.5124	0.3066	2.3719
Ideal point	—	—	—	0.7302	6.7567	0.9474	0.1093
Nonideal point	—	—	—	0.0553	1.0220	−13.717	14.214

results obtained in the last section and validates the optimization algorithm. However, different values of the current density in the outputs are due to the differences between the decision-making methods. There is no other means to judge which one is better. However, the results can be compared, as in the next section.

4.4 | Sensitivity analysis

Finally, to compare the results of the different decision-making methods and the different proposed scenarios, and also to make sure the answers are the best possible ones, in this section, the sensitivity of the objective functions to the decision variables is computed. Tables 6 and 7 address the sensitivity of the objective functions at the optimum points at the operating temperature of the MCFC and the thermal conductance, respectively. Four current densities are selected. They include the current densities of 1000, 1359, 1602, and 4653 (A m^{-2}). These points are those which approximately optimize one of the objective functions individually.

According to Table 6, with 2.21% increase in the working temperature of the MCFC (from 905 to 925 K), the energy efficiency increases by 0.73%, 1.39%, 1.86%, and 15.42% at current densities of 1000, 1359, 1602, and 4653 (A m^{-2}), respectively; The fresh water production rate increases by 1.06%, 1.55%, 1.99%, and 15.41% at the different current densities mentioned above, respectively; The exergy destruction rate density decreases by 25.47%, 14.10%, 12.37%, and 12.88%, respectively; Finally, the ecological function density increases by 5.80%, 9.17%, 12.62%, and 39.43%,

TABLE 6 The objective functions variations with the operating temperature of the MCFC for $\theta = 1000$ (W K^{-1}) at optimum values of j

j (A m^{-2})	T (K)	η_H	$\dot{m}_p$ (m^3 s^{-1})	exd_H (kW m^{-2})	e_H (kW m^{-2})
1000	905	0.7134	1.88	146.62	768.18
	925	0.7186	1.90	109.28	812.70
1359	905	0.7198	2.58	419.38	834.92
	925	0.7298	2.62	360.23	911.52
1602	905	0.7154	3.02	633.28	836.31
	925	0.7287	3.08	554.92	941.85
4653	905	0.4650	5.71	5731.88	−2957.76
	925	0.5367	6.59	4993.64	−1791.61

j (A m^{-2})	θ	η_H	$\dot{m}_p$ (m^3 s^{-1})	exd$_H$ (kW m^{-2})	e_H (kW m^{-2})
1000	900	0.7163	1.89	127.27	791.15
	1100	0.7163	1.89	127.19	791.33
1359	900	0.7250	2.60	388.86	874.42
	1100	0.7254	2.60	388.05	876.03
1602	900	0.7220	3.05	593.14	890.03
	1100	0.7229	3.06	591.29	893.73
4653	900	0.4924	6.05	5404.83	−2467.23
	1100	0.5128	6.30	5282.83	−2223.23

TABLE 7 The objective functions variations with the thermal conductance for $T = 915$ (K) at optimum values of j

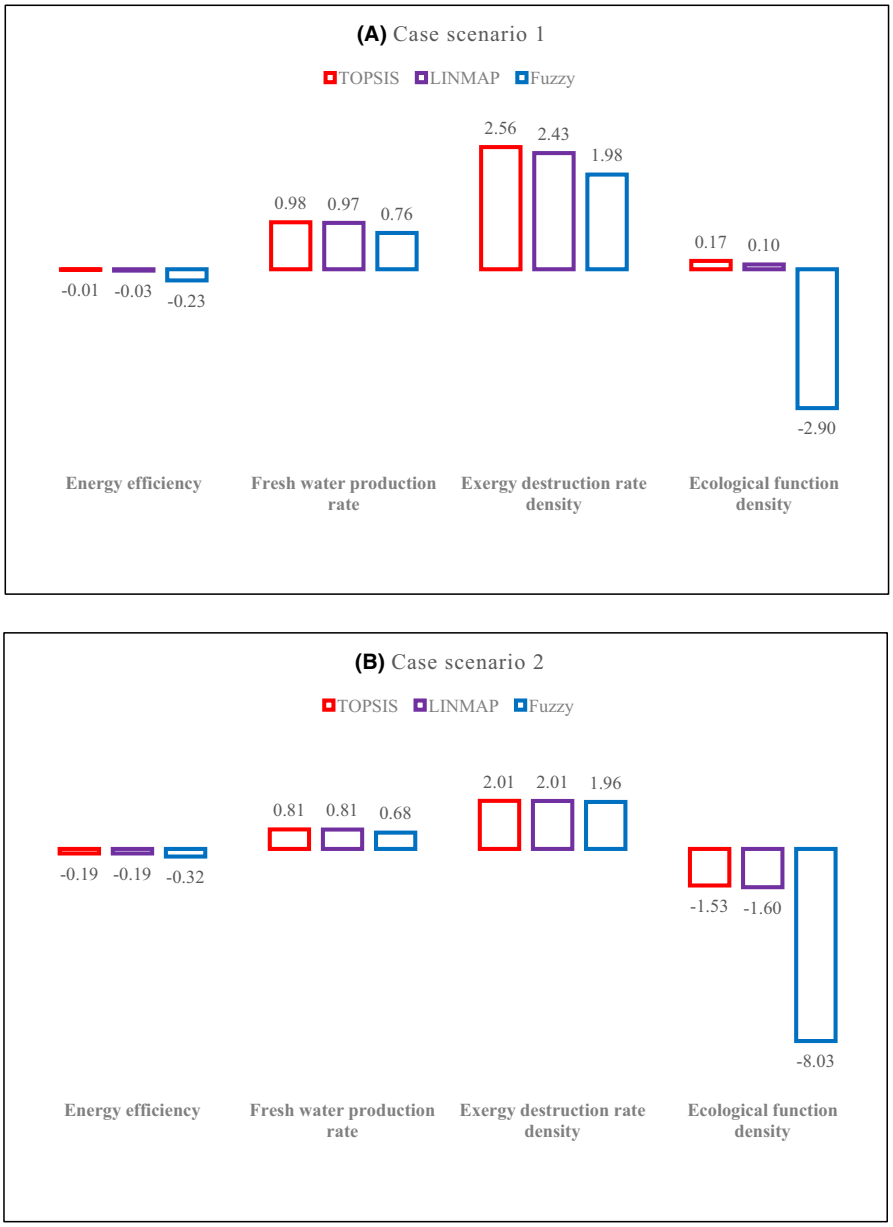

FIGURE 4 Variation of the objective functions with 1% increase in current density at the proposed points by the decision-making methods in the two proposed case scenarios

respectively. This shows that the most influenced objective function is the ecological function density and the sensitivity also increases with the increase in the current density in the three objective functions including the energy efficiency, fresh water production rate, and the ecological function density. However, the sensitivity of the exergy destruction rate density has the opposite behavior. It is maximum at first (at $j = 1000$ (A m^{-2})) where the function itself is also optimum.

Then it decreases until where the ecological function is nearly maximized and finally increases again at $j = 4653$ (A m^{-2}).

According to Table 7, with an increase of 22.22% in the thermal conductance (from 900 to 1100 (W K^{-1})), the energy efficiency virtually stays constant at $j = 1000$ (A m^{-2}), and increases by 0.06%, 0.12%, and 4.14% at $j = 1359$, 1602, and 4653 (A m^{-2}), respectively; The fresh water production rate, also, does not change at $j = 1000$ and 1359 (A m^{-2}), but increases by 0.33 and 4.13% at $j = 1602$ and 4653 (A m^{-2}), respectively. The exergy destruction rate always increases by the increase in the thermal conductance and these increases augment with the increase in the current density. It increases by 0.06%, 0.21%, 0.31%, and 2.26% at $j = 1000$, 1359, 1602, and 4653, respectively, with an increase of 22.22% in the thermal conductance. Finally, the ecological function sensitivity to the thermal conductance increases with the increase in the current density and it increases by 0.02%, 0.18%, 0.42%, and 9.89% with an increase of 22.22% in the thermal conductance at the current densities mentioned above, respectively. These results also show that the most influential decision variable is the current density of the FC. Figure 4 shows what percent each decision variable changes along with an increase of 1% in the current density in different scenarios, at selected points by the different decision-making methods.

5 | CONCLUSIONS

A detailed thermodynamic analysis is conducted in this study in trying to study the performance of a hybrid cycle consisting of an MCFC and a Stirling engine which drives high pressure pumps of a reverse osmosis desalination system to produce fresh water. After studying the characteristic curves of the cycle, two triple-objective optimization approaches are implemented; each considering a combination of the desired objective functions. Three well-known and powerful decision-making methods, including TOPSIS, LINMAP, and Fuzzy, are employed to select the final outcomes from the Pareto fronts obtained by the Genetic algorithm. In the first scenario which considers the energy efficiency, fresh water production rate and the exergy destruction rate density, the energy efficiency has a better condition in the TOPSIS approach. It meets its maximum, 0.7299, which is 99.96% of its ideal value; the fresh water production rate reaches its optimum value in the Fuzzy approach, 5.07 (m^3 s^{-1}) which is 74.98% of its ideal value; and the exergy destruction rate density is at its optimum value in the TOPSIS approach, 0.48 (kW m^{-2}) which is 341.35% more than its ideal value which is 0.11 (kW m^{-2}). In the second scenario which include the energy efficiency, fresh water production rate and the ecological function density, the energy efficiency meets its maximum again in the TOPSIS results, 0.6962, which is 95.34% of its ideal value; the fresh water production rate is at its peak in the Fuzzy results, again, which is 5.51 (m^3 s^{-1}), 81.58% of its ideal value; the ecological function density reaches its maximum in the TOPSIS results, 0.77 (kW m^{-2}), which is 80.93% of its ideal value. Finally, a sensitivity analysis is performed indicating what percent the final outputs of each decision-making method changes due to changes in the decision variables, in different conditions.

ACKNOWLEDGMENTS

This research was supported by the National Natural Science Foundation of China (Grant No. 51778511), Hubei Provincial Natural Science Foundation of China (Grant No. 2018CFA029), Key Project of ESI Discipline Development of Wuhan University of Technology (Grant No. 2017001), and the Scientific Research Foundation of Wuhan University of Technology (Grant No. 40120237).

ORCID

Mohammad H. Ahmadi https://orcid.org/0000-0002-0097-2534
Mohammad Sameti https://orcid.org/0000-0001-9365-0157
Fathollah Pourfayaz https://orcid.org/0000-0001-6297-9603
Mohammad Ali Jokar https://orcid.org/0000-0001-9265-4252

REFERENCES

1. Ahmadi MH, Ahmadi MA, Mellit A, Pourfayaz F, Feidt M. Thermodynamic analysis and multi objective optimization of performance of solar dish Stirling engine by the centrality of entransy and entropy generation. *Int J Electr Power Energy Syst*. 2016;78:88-95.
2. Badescu V. Optimizing of Stirling and Ericsson cycles using solar radiation. *Space Power*. 1992;11(2):99-106.
3. Kongtragool B, Wongwises S. A review of solar-powered Stirling engines and low temperature differential Stirling engines. *Renew Sustain Energy Rev*. 2003;7(2):131-154.
4. Liao T, Lin J. Optimum performance characteristics of a solar-driven Stirling heat engine system. *Energy Convers Manage*. 2015;97:20-25.
5. Poullikkas A, Kourtis G, Hadjipaschalis I. Parametric analysis for the installation of solar dish technologies in Mediterranean regions. *Renew Sustain Energy Rev*. 2010;14(9):2772-2783.
6. Klaiß H, Köhne R, Nitsch J, Sprengel U. Solar thermal power plants for solar countries—technology, economics and market potential. *Appl Energy*. 1995;52(2):165-183.

7. Das DC, Sinha N, Roy A. Small signal stability analysis of dish-Stirling solar thermal based autonomous hybrid energy system. *Int J Electr Power Energy Syst*. 2014;63:485-498.
8. Mancini T, Heller P, Butler B, et al. Dish-Stirling systems: an overview of development and status. *J Sol Energy Eng*. 2003;125(2):135-151.
9. Howard DF, Liang J, Harley RG. Control of receiver temperature and shaft speed in dish-Stirling solar power plants to meet grid integration requirements. In Energy Conversion Congress and Exposition (ECCE), 2010 IEEE.
10. Santos-Martin D, Alonso-Martinez J, Eloy-Garcia J, Arnalte S. Solar dish-Stirling system optimisation with a doubly fed induction generator. *IET Renew Power Gener*. 2012;6(4):276-288.
11. Lund K. *Applications of Finite-time Thermodynamics to Solar Power Conversion. Finite-time Thermodynamics and Thermoeconomics*. London: Taylor & Francis, 1990: 121.
12. Angulo-Brown F. An ecological optimization criterion for finite-time heat engines. *J Appl Phys*. 1991;69(11):7465-7469.
13. Chen J. Optimization of a solar-driven heat engine. *J Appl Phys*. 1992;72(8):3778-3780.
14. Ladas HG, Ibrahim O. Finite-time view of the Stirling engine. *Energy*. 1994;19(8):837-843.
15. Blank DA, Davis GW, Wu C. Power optimization of an endoreversible Stirling cycle with regeneration. *Energy*. 1994;19(1):125-133.
16. Tun SG. Finite-time optimization of a solar-driven heat engine. *Sol Energy*. 1996;56(6):617-620.
17. Trukhow VS, Tursunbaev IA, Lezhebokov IA, Kenzhaev IG. Energy balance of autonomous solar power plant with the Stirling engine. *Appl Solar Energy*. 1997;33(1):17-23.
18. Chen J, Yan Z, Chen L, Andresen B. Efficiency bound of a solar-driven Stirling heat engine system. *Int J Energy Res*. 1998;22(9):805-812.
19. Kaushik S, Kumar S. Finite time thermodynamic analysis of endoreversible Stirling heat engine with regenerative losses. *Energy*. 2000;25(10):989-1003.
20. Sahin AZ. Finite-time thermodynamic analysis of a solar driven heat engine. *Exergy Int J*. 2001;1(2):122-126.
21. Kaushik S, Kumar S. Finite time thermodynamic evaluation of irreversible Ericsson and Stirling heat engines. *Energy Convers Manage*. 2001;42(3):295-312.
22. He J, Chen J, Wu C. Ecological optimisation of an irreversible Stirling heat engine. *Int J Ambient Energy*. 2001;22(4):211-220.
23. Sahin B, Kodal A. Performance analysis of an endoreversible heat engine based on a new thermoeconomic optimization criterion. *Energy Convers Manage*. 2001;42(9):1085-1093.
24. Yilmaz T, Ust Y, Erdil A. Optimum operating conditions of irreversible solar driven heat engines. *Renew Energ*. 2006;31(9):1333-1342.
25. Sharma A, Shukla SK, Rai KA. Finite time thermodynamic analysis and optimization of solar-dish Stirling heat engine with regenerative losses. *Thermal Sci*. 2011;15(4):995-1009.
26. Yaqi L, Yaling H, Weiwei W. Optimization of solar-powered Stirling heat engine with finite-time thermodynamics. *Renew Energ*. 2011;36(1):421-427.
27. Sameti M, Jokar MA, Astaraei FR. Prediction of solar Stirling power generation in smart grid by GA-ANN model. *Int J Comput Appl Technol*. 2017;55(2):147-157.
28. Zhao Y, Ou C, Chen J. A new analytical approach to model and evaluate the performance of a class of irreversible fuel cells. *Int J Hydrogen Energy*. 2008;33(15):4161-4170.
29. Zhang X, Guo J, Chen J. The parametric optimum analysis of a proton exchange membrane (PEM) fuel cell and its load matching. *Energy*. 2010;35(12):5294-5299.
30. Zhang H, Lin G, Chen J. Performance analysis and multi-objective optimization of a new molten carbonate fuel cell system. *Int J Hydrogen Energy*. 2011;36(6):4015-4021.
31. Zhang H, Lin G, Chen J. Multi-objective optimisation analysis and load matching of a phosphoric acid fuel cell system. *Int J Hydrogen Energy*. 2012;37(4):3438-3446.
32. Zhang H, Chen L, Zhang J, Chen J. Performance analysis of a direct carbon fuel cell with molten carbonate electrolyte. *Energy*. 2014;68:292-300.
33. Chen X, Li W, Gong G, Wan Z, Tu Z. Parametric analysis and optimization of PEMFC system for maximum power and efficiency using MOEA/D. *Appl Therm Eng*. 2017;121:400-409.
34. Ahmadi MH, Ahmadi M-A, Maleki A, Pourfayaz F, Bidi M, Açıkkalp E. Exergetic sustainability evaluation and multi-objective optimization of performance of an irreversible nanoscale Stirling refrigeration cycle operating with Maxwell–Boltzmann gas. *Renew Sustain Energy Rev*. 2017;78:80-92.
35. Zhang X, Chen J. Performance analysis and parametric optimum criteria of a class of irreversible fuel cell/heat engine hybrid systems. *Int J Hydrogen Energy*. 2010;35(1):284-293.
36. Chen X, Chen L, Guo J, Chen J. An available method exploiting the waste heat in a proton exchange membrane fuel cell system. *Int J Hydrogen Energy*. 2011;36(10):6099-6104.
37. Zhang H, Lin G, Chen J. Performance evaluation and parametric optimum criteria of an irreversible molten carbonate fuel cell-heat engine hybrid system. *Int J Electrochem Sci*. 2011;6(10):4714-4729.
38. Zhang X, Su S, Chen J, Zhao Y, Brandon N. A new analytical approach to evaluate and optimize the performance of an irreversible solid oxide fuel cell-gas turbine hybrid system. *Int J Hydrogen Energy*. 2011;36(23):15304-15312.
39. Zhang X, Guo J, Chen J. Influence of multiple irreversible losses on the performance of a molten carbonate fuel cell-gas turbine hybrid system. *Int J Hydrogen Energy*. 2012;37(10):8664-8671.
40. Chen L, Gao S, Zhang H. Performance analysis and multi-objective optimization of an irreversible solid oxide fuel cell-stirling heat engine hybrid system. *Int J Electrochem Sci*. 2013;8:10772-10787.
41. Chen L, Zhang H, Gao S, Yan H. Performance optimum analysis of an irreversible molten carbonate fuel cell–Stirling heat engine hybrid system. *Energy*. 2014;64:923-930.
42. Zhang X, Wang Y, Guo J, Shih T-M, Chen J. A unified model of high-temperature fuel-cell heat-engine hybrid systems and analyses of its optimum performances. *Int J Hydrogen Energy*. 2014;39(4):1811-1825.
43. Zhao M, Zhang H, Hu Z, Zhang Z, Zhang J. Performance characteristics of a direct carbon fuel cell/thermoelectric generator hybrid system. *Energy Convers Manage*. 2015;89:683-689.
44. Yang P, Zhang H. Parametric analysis of an irreversible proton exchange membrane fuel cell/absorption refrigerator hybrid system. *Energy*. 2015;85:458-467.

45. Chen X, Wang Y, Cai L, Zhou Y. Maximum power output and load matching of a phosphoric acid fuel cell-thermoelectric generator hybrid system. *J Power Sources*. 2015;294:430-436.
46. Zhang X, Liu H, Ni M, Chen J. Performance evaluation and parametric optimum design of a syngas molten carbonate fuel cell and gas turbine hybrid system. *Renew Energ*. 2015;80:407-414.
47. Yang Z, Liao T, Zhou Y, Lin G, Chen J. Performance evaluation and parametric optimum design of a molten carbonate fuel cell-thermophotovoltaic cell hybrid system. *Energy Convers Manage*. 2016;128:28-33.
48. Huang C, Pan Y, Wang Y, Su G, Chen J. An efficient hybrid system using a thermionic generator to harvest waste heat from a reforming molten carbonate fuel cell. *Energy Convers Manage*. 2016;121:186-193.
49. Yang P, Zhang H, Hu Z. Parametric study of a hybrid system integrating a phosphoric acid fuel cell with an absorption refrigerator for cooling purposes. *Int J Hydrogen Energy*. 2016;41(5):3579-3590.
50. Chen X, Wang Y, Zhao Y, Zhou Y. A study of double functions and load matching of a phosphoric acid fuel cell/heat-driven refrigerator hybrid system. *Energy*. 2016;101:359-365.
51. Ye Z, Zhang X, Li W, Su G, Chen J. Optimum operation states and parametric selection criteria of a high temperature fuel cell-thermoradiative cell system. *Energy Convers Manage*. 2018;173:470-475.
52. Van Veldhuizen DA, Lamont GB. Multiobjective evolutionary algorithms: analyzing the state-of-the-art. *Evol Comput*. 2000;8(2):125-147.
53. Konak A, Coit DW, Smith AE. Multi-objective optimization using genetic algorithms: a tutorial. *Reliab Eng Syst Safe*. 2006;91(9):992-1007.
54. Bäck T, Fogel D, Michalewicz Z. *Handbook of Evolutionary Computation Release 97/1*. Oxford, UK: Oxford University Press; 1997:B1.
55. Lazzaretto A, Toffolo A. Energy, economy and environment as objectives in multi-criterion optimization of thermal systems design. *Energy*. 2004;29(8):1139-1157.
56. Zhang J, Zhu H, Yang C, Li Y, Wei H. Multi-objective shape optimization of helico-axial multiphase pump impeller based on NSGA-II and ANN. *Energy Convers Manage*. 2011;52(1):538-546.
57. Ahmadi MH, Hosseinzade H, Sayyaadi H, Mohammadi AH, Kimiaghalam F. Application of the multi-objective optimization method for designing a powered Stirling heat engine: design with maximized power, thermal efficiency and minimized pressure loss. *Renew Energ*. 2013;60:313-322.
58. Ahmadi MH, Sayyaadi H, Dehghani S, Hosseinzade H. Designing a solar powered Stirling heat engine based on multiple criteria: maximized thermal efficiency and power. *Energy Convers Manage*. 2013;75:282-291.
59. Ahmadi MH, Sayyaadi H, Mohammadi AH, Barranco-Jimenez MA. Thermo-economic multi-objective optimization of solar dish-Stirling engine by implementing evolutionary algorithm. *Energy Convers Manage*. 2013;73:370-380.
60. Wang J, Yan Z, Wang M, Li M, Dai Y. Multi-objective optimization of an organic Rankine cycle (ORC) for low grade waste heat recovery using evolutionary algorithm. *Energy Convers Manage*. 2013;71:146-158.
61. Ahmadi MH, Dehghani S, Mohammadi AH, Feidt M, Barranco-Jimenez MA. Optimal design of a solar driven heat engine based on thermal and thermo-economic criteria. *Energy Convers Manage*. 2013;75:635-642.
62. Ahmadi MH, Mohammadi AH, Dehghani S, Barranco-Jiménez MA. Multi-objective thermodynamic-based optimization of output power of Solar Dish-Stirling engine by implementing an evolutionary algorithm. *Energy Convers Manage*. 2013;75:438-445.
63. Toghyani S, Kasaeian A, Ahmadi MH. Multi-objective optimization of Stirling engine using non-ideal adiabatic method. *Energy Convers Manage*. 2014;80:54-62.
64. Ahmadi MH, Ahmadi MA, Mohammadi AH, Feidt M, Pourkiaei SM. Multi-objective optimization of an irreversible Stirling cryogenic refrigerator cycle. *Energy Convers Manage*. 2014;82:351-360.
65. Ahmadi MH, Ahmadi M-A, Mohammadi AH, Mehrpooya M, Feidt M. Thermodynamic optimization of Stirling heat pump based on multiple criteria. *Energy Convers Manage*. 2014;80:319-328.
66. Ahmadi MH, Ahmadi M-A, Mehrpooya M, Hosseinzade H, Feidt M. Thermodynamic and thermo-economic analysis and optimization of performance of irreversible four-temperature-level absorption refrigeration. *Energy Convers Manage*. 2014;88:1051-1059.
67. Sayyaadi H, Ahmadi MH, Dehghani S. Optimal design of a solar-driven heat engine based on thermal and ecological criteria. *J Energy Eng*. 2014;141(3):04014012.
68. Sahraie H, Mirani MR, Ahmadi MH, Ashouri M. Thermo-economic and thermodynamic analysis and optimization of a two-stage irreversible heat pump. *Energy Convers Manage*. 2015;99:81-91.
69. Ahmadi MH, Ahmadi MA, Bayat R, Ashouri M, Feidt M. Thermo-economic optimization of Stirling heat pump by using non-dominated sorting genetic algorithm. *Energy Convers Manage*. 2015;91:315-322.
70. Ahmadi MH, Ahmadi MA. Thermodynamic analysis and optimization of an irreversible Ericsson cryogenic refrigerator cycle. *Energy Convers Manage*. 2015;89:147-155.
71. Ahmadi MH, Ahmadi MA, Mehrpooya M, Sameti M. Thermo-ecological analysis and optimization performance of an irreversible three-heat-source absorption heat pump. *Energy Convers Manage*. 2015;90:175-183.
72. Ahmadi MH, Ahmadi M-A, Feidt M. Thermodynamic analysis and evolutionary algorithm based on multi-objective optimization of performance for irreversible four-temperature-level refrigeration. *Mech Ind*. 2015;16(2):207.
73. Sadatsakkak SA, Ahmadi MH, Bayat R, Pourkiaei SM, Feidt M. Optimization density power and thermal efficiency of an endoreversible Braysson cycle by using non-dominated sorting genetic algorithm. *Energy Convers Manage*. 2015;93:31-39.
74. Sadatsakkak SA, Ahmadi MH, Ahmadi MA. Thermodynamic and thermo-economic analysis and optimization of an irreversible regenerative closed Brayton cycle. *Energy Convers Manage*. 2015;94:124-129.
75. Ahmadi MH, Ahmadi MA, Sadatsakkak SA. Thermodynamic analysis and performance optimization of irreversible Carnot

refrigerator by using multi-objective evolutionary algorithms (MOEAs). *Renew Sustain Energy Rev*. 2015;51:1055-1070.
76. Ahmadi MH, Mehrpooya M. Thermo-economic modeling and optimization of an irreversible solar-driven heat engine. *Energy Convers Manage*. 2015;103:616-622.
77. Ahmadi MH, Ahmadi M-A, Pourfayaz F. Performance assessment and optimization of an irreversible nano-scale Stirling engine cycle operating with Maxwell-Boltzmann gas. *Eur Phys J Plus*. 2015;130(9):1-13.
78. Ahmadi MH, Ahmadi M-A, Pourfayaz F, Bidi M. Thermodynamic analysis and optimization for an irreversible heat pump working on reversed Brayton cycle. *Energy Convers Manage*. 2016;110:260-267.
79. Ahmadi MH, Ahmadi MA, Shafaei A, Ashouri M, Toghyani S. Thermodynamic analysis and optimization of the Atkinson engine by using NSGA-II. *Int J Low-Carbon Technol*. 2016;11(3):317-324.
80. Pirkandi J, Jokar MA, Sameti M, Kasaeian A, Kasaeian F. Simulation and multi-objective optimization of a combined heat and power (CHP) system integrated with low-energy buildings. *J Build Eng*. 2016;5:13-23.
81. Ahmadi MH, Ahmadi MA, Pourfayaz F. Thermodynamic analysis and evolutionary algorithm based on multi-objective optimization performance of actual power generating thermal cycles. *Appl Therm Eng*. 2016;99:996-1005.
82. Ahmadi MH, Ahmadi M-A, Mehrpooya M, Feidt M, Rosen MA. Optimal design of an Otto cycle based on thermal criteria. *Mech Ind*. 2016;17(1):111.
83. Ahmadi MH, Mohammadi AH, Pourkiaei SM. Optimisation of the thermodynamic performance of the Stirling engine. *Int J Ambient Energy*. 2016;37(2):149-161.
84. Ahmadi MH, Ahmadi MA. Multi objective optimization of performance of three-heat-source irreversible refrigerators based algorithm NSGAII. *Renew Sustain Energy Rev*. 2016;60:784-794.
85. Ahmadi MH, Ahmadi MA, Feidt M. Performance optimization of a solar-driven multi-step irreversible brayton cycle based on a multi-objective genetic algorithm. *Oil Gas Sci Technol–Revue d'IFP Energies nouvelles*. 2016;71(1):16.
86. Arora R, Kaushik SC, Kumar R, Arora R. Multi-objective thermo-economic optimization of solar parabolic dish Stirling heat engine with regenerative losses using NSGA-II and decision making. *Int J Electr Power Energy Syst*. 2016;74:25-35.
87. Wong JY, Sharma S, Rangaiah G. Design of shell-and-tube heat exchangers for multiple objectives using elitist non-dominated sorting genetic algorithm with termination criteria. *Appl Therm Eng*. 2016;93:888-899.
88. Hoseini Rahdar M, Heidari M, Ataei A, Choi J-K. Modeling and optimization of R-717 and R-134a ice thermal energy storage air conditioning systems using NSGA-II and MOPSO algorithms. *Appl Therm Eng*. 2016;96:217-227.
89. Ahmadi MH, Amin Nabakhteh M, Ahmadi M-A, Pourfayaz F, Bidi M. Investigation and optimization of performance of nano-scale Stirling refrigerator using working fluid as Maxwell–Boltzmann gases. *Phys A Stat Mech Appl*. 2017;483:337-350.
90. Ahmadi MH, Mehrpooya M, Abbasi S, Pourfayaz F, Bruno JC. Thermo-economic analysis and multi-objective optimization of a transcritical CO2 power cycle driven by solar energy and LNG cold recovery. *Thermal Sci Eng Prog*. 2017;4:185-196.
91. Açıkkalp E. Ecologic and sustainable objective thermodynamic evaluation of molten carbonate fuel cell–supercritical CO_2 Brayton cycle hybrid system. *Int J Hydrogen Energy*. 2017;42(9):6272-6280.
92. Bahari SS, Sameti M, Ahmadi MH, Haghgooyan MS. Optimisation of a combined Stirling cycle–organic Rankine cycle using a genetic algorithm. *Int J Ambient Energy*. 2016;37(4):398-402.
93. El-Dessouky HT, Ettouney HM. *Fundamentals of Salt Water Desalination*. Amsterdam, Netherlands: Elsevier; 2002.
94. Deb K, Pratap A, Agarwal S, Meyarivan T. A fast and elitist multiobjective genetic algorithm: NSGA-II. *IEEE Trans Evol Comput*. 2002;6(2):182-197.
95. Zhou A, Qu B-Y, Li H, Zhao S-Z, Suganthan PN, Zhang Q. Multiobjective evolutionary algorithms: a survey of the state of the art. *Swarm Evolut Comput*. 2011;1(1):32-49.
96. Xia G, Sun Q, Cao X, Wang J, Yu Y, Wang L. Thermodynamic analysis and optimization of a solar-powered transcritical CO_2 (carbon dioxide) power cycle for reverse osmosis desalination based on the recovery of cryogenic energy of LNG (liquefied natural gas). *Energy*. 2014;66:643-653.
97. Jokar MA, Ahmadi MH, Sharifpur M, Meyer JP, Pourfayaz F, Ming T. Thermodynamic evaluation and multi-objective optimization of molten carbonate fuel cell-supercritical CO_2 Brayton cycle hybrid system. *Energy Convers Manage*. 2017;153:538-556.
98. Açıkkalp E. Performance analysis of irreversible molten carbonate fuel cell–Braysson heat engine with ecological objective approach. *Energy Convers Manage*. 2017;132:432-437.
99. Açıkkalp E. Thermo-environmental performance analysis of irreversible solid oxide fuel cell–Stirling heat engine. *Int J Ambient Energy*. 2017;39:751-758.
100. Ahmadi MH, Jokar MA, Ming T, Feidt M, Pourfayaz F, Astaraei FR. Multi-objective performance optimization of irreversible molten carbonate fuel cell–Braysson heat engine and thermodynamic analysis with ecological objective approach. *Energy*. 2018;144:707-722.

How to cite this article: Ahmadi MH, Sameti M, Pourkiaei SM, et al. Multi-objective performance optimization of irreversible molten carbonate fuel cell–Stirling heat engine–reverse osmosis and thermodynamic assessment with ecological objective approach. *Energy Sci Eng*. 2018;6:783–796. https://doi.org/10.1002/ese3.252